Thomson-Scattering Measurements of Ion-Acoustic Fluctuations in CO_2-Laser–Plasma Interaction

F. Martin
Institut Nacional de la Recherche Scientifique–Energie, Varennes, Québec, J0L 2P0, Canada

and

H. A. Baldis and C. J. Walsh
Division of Physics, National Research Council, Ottawa, Ontario, K1A 0R6, Canada
(Received 11 October 1983)

Space- and time-resolved Thomson scattering has been used to characterize strong nonthermal ion-acoustic fluctuations in CO_2-laser–heated plasmas in the density range $0.3 \leq n/n_c \leq 2.0$. The relative fluctuation amplitude scales as $\delta n/n \sim I^{0.6}$ with a level of $\delta n/n \simeq 15\%$ at a laser intensity $I = 2.3 \times 10^{14}$ W/cm^2. No saturation with intensity is observed. The wave-number spectrum peaks at a constant $k\lambda_D \simeq 0.12$ over all densities.

PACS numbers: 52.35.Mw

In laser-plasma interaction experiments, ion-acoustic fluctuations are generated from the ion-acoustic drift instability[1] when the electron drift velocity exceeds the ion-acoustic velocity ($u \geq c_s$) and $ZT_e/T_i \geq 3$ where T_e and T_i are the electron and ion temperature and Z the plasma ionization state. These fluctuations have been invoked to explain nonclassical plasma behavior in absorption of laser radiation,[2-5] generation of energetic ions and electrons,[4,5] and heat transport of the absorbed energy.[6,7] The magnitude of these effects depends critically on the saturation level of the ion wave and on the wave-number spectrum. Theoretical estimates[3-7] for the saturation level cover two orders of magnitude in fluctuation amplitude ($10^{-3} \leq \delta n/n \leq 10^{-1}$). High fluctuation levels ($\delta n/n \simeq 0.1$) have been measured[8,9] at selected values of plasma density and wave number.

This Letter reports the first laser Thomson-scattering measurements to characterize simultaneously, on a single event, the spatial and temporal characteristics of ion-acoustic turbulence along a density gradient. A preformed plasma produced by a 4-J, 30-nsec, 1.06-μm laser pulse on a carbon target is irradiated with a high-intensity CO_2 laser (40 J, 1 nsec, $d \simeq 150$ μm) pulse along the density gradient (Fig. 1). As in earlier experiments,[9] background plasma parameters are $T_e \simeq 100$ eV, $Z \simeq 3-4$, $(n^{-1}dn/dx)^{-1} \simeq 300$ μm. Forward scattering ($\theta_s \simeq 20°$) is used to probe wave vectors $\vec{k}_s$ parallel to the density gradient ($\vec{k}_s \| \nabla n_e \| \vec{k}_{CO_2}$) covering the wave-number range 2.5×10^4 cm$^{-1} \leq k_s \leq 7.0 \times 10^4$ cm^{-1} which corresponds to $0.06 \leq k_s \lambda_D \leq 0.16$ for a 100-eV plasma at n_c. The incident probe beam (0.53 μm) is brought to a line focus (600×100 μm^2) parallel to the scattering wave vector (Fig. 1). The center of the line focus is positioned at n_c so that the scattering volume covers $0.3 \leq n/n_c \leq 2.0$ in density. A streak camera records the scattered signal as a function of position and time (Fig. 2). The scattering geometry is such as not to collect any light scattered by ion waves generated by

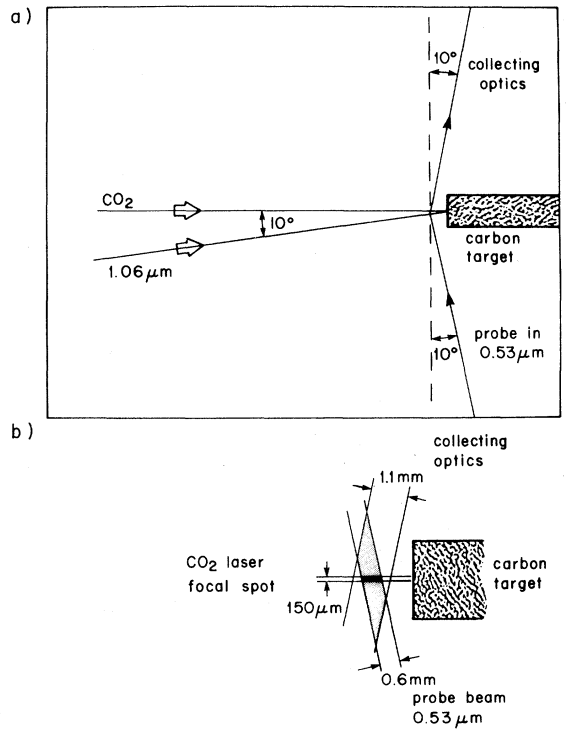

FIG. 1. Diagram of experiment and Thomson-scattering geometry showing the carbon target, the laser beam which produces the plasma ($\lambda = 1.06$ μm), and the CO_2 heating-laser beam incident at 90° to the target. The electric field of the CO_2 laser is in the scattering plane. The scattering illumination geometry and the plasma volume imaged by the collection optics are shown in (b).

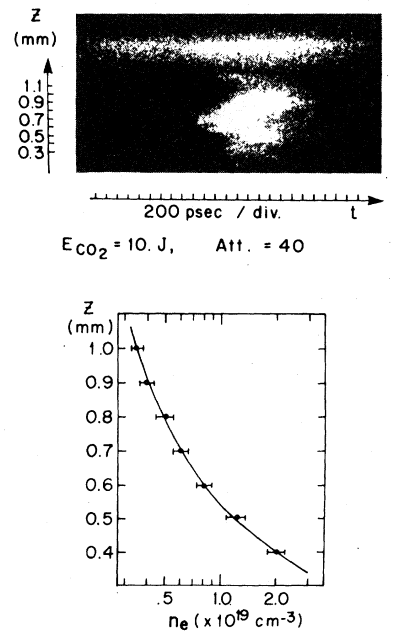

FIG. 2. Scattered signal as a function of distance from target (z) and time (t) as seen at the output of the streak camera. Attenuation (Att.) of the scattered signal is also indicated. The upper trace is the probe beam used to normalize the scattered power. The streak camera is triggered by the electrical pulse from the CO_2 shaping Pockels cells. This ensures a jitter less than 50 psec in the triggering of the streak camera with respect to the CO_2 laser pulse and allows time correlation between different shots. The associated measured background density profile is shown below.

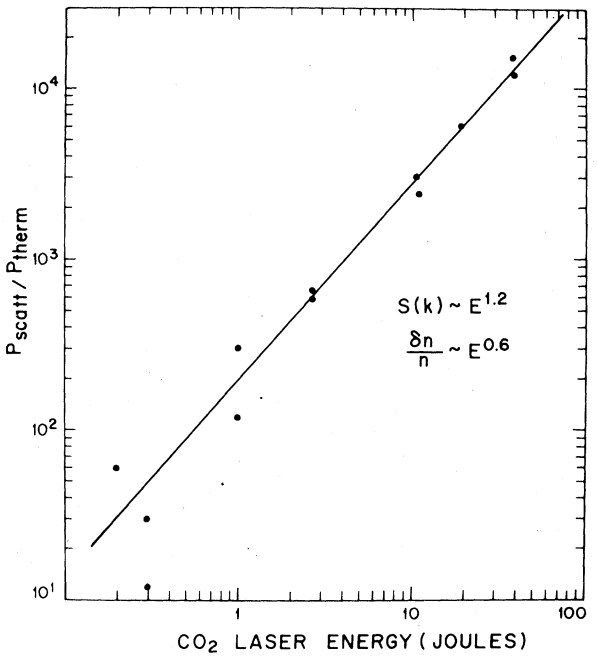

FIG. 3. Dependence of scattered power on CO_2 laser energy. The scattered signal is normalized to the signal scattered from the thermal fluctuations of the plasma in the absence of the CO_2 laser.

stimulated Brillouin scattering[10] ($k_s = 2k_{CO_2} = 1.2\times10^4$ cm^{-1}). The wave-number dependence of the scattered radiation is measured by masking the collection optics with a 1-mm slit to define the collection angle.

The thermal scattering level (no CO_2) is measured and used as a reference. The thermal fluctuation level (no CO_2) corresponding to wave vectors in the scattering range is[9] $[\delta n/n]_{\text{thermal}} = 1.3\times10^{-4}$ at n_c. Interferometry of the preformed plasma using a 2-nsec, 0.53-μm probe provides the density distribution of each event (Fig. 2). We make the logical assumption that the enhanced fluctuations are localized in the CO_2 focal spot.

The enhancement of scattered signal over thermal is given in Fig. 3 as a function of incident laser energy. Scattered power P_s/P_{th} scales as $E^{1.2}$ with energy so that $\delta n/n \sim E^{0.6}$ with no sign of saturation. Parametric decay[10] cannot account for the observed fluctuations because the scattering vector is normal to the CO_2 laser electric field. A more likely candidate is current-driven ion-acoustic turbulence.[1,2]

Time evolution of scattered power as a function of incident energy and position (density) is given in Fig. 4. One should keep in mind that the fluctuation level is increasing with energy (Fig. 3). Several points are worth noting. Fluctuations tend to start near n_c. Fluctuations start sooner and spread out faster at high laser energy. Fluctuation lifetime is greater than the laser pulse width at low energies. This is consistent with an indirectly driven instability like the current-driven ion-acoustic instability. A similar time dependence for T_e was observed by Gray *et al.*[8] at these flux levels. Their explanation was based on heat-transport inhibition. Considering a simple model where heat flux inhibition is caused by an anomalous collision frequency[6] which is proportional to $(\delta n/n)^2$, one would expect the increased inhibition at high laser energy to maintain the T_e differential for a longer time so that the fluctuation lifetime should be longer than at low laser energy. In fact, the fluctuation lifetime [Fig. 4(b)] decreases at higher laser intensity to a lower limit set by the laser pulse width indicating increased damping presumably by enhanced generation of fast ions, predicted by theory[5] at a fluctuation level of $\delta n/n \simeq 10^{-3}$.

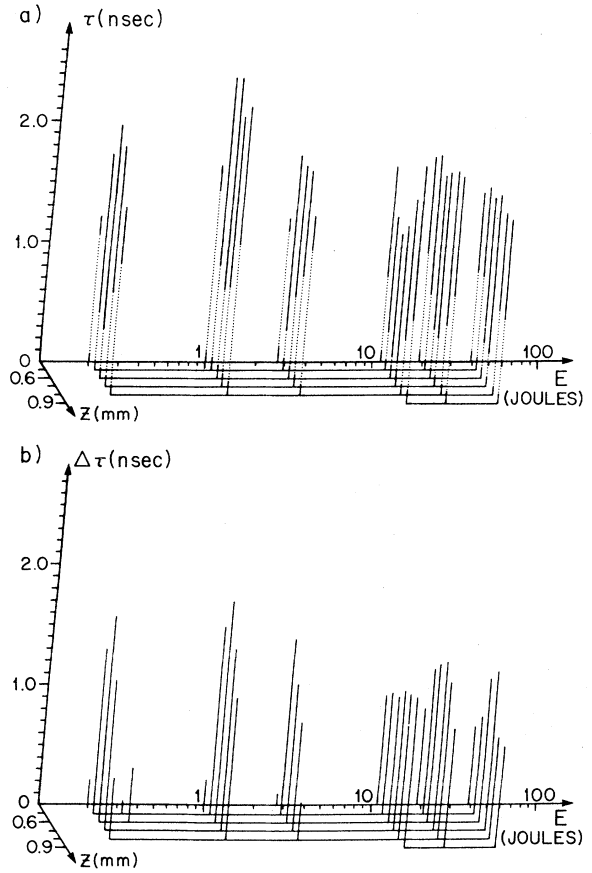

FIG. 4. Dependence (a) of the onset and termination in time of the scattered signal and (b) of the time duration of the scattered signal on axial position (z) and CO_2 laser energy (E). Axial position is related to density by Fig. 2. The data represent an average over two shots at each laser energy.

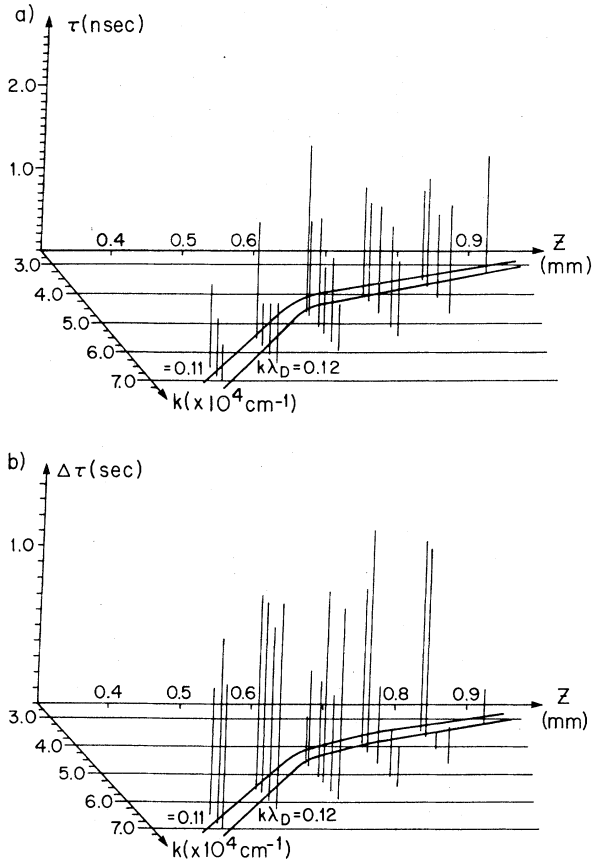

FIG. 5. Dependence (a) of the onset in time of the scattered signal and (b) of the time duration of the scattered signal on axial position (z) and fluctuation wave number (k). Constant $k\lambda_D$ curves are drawn in the k-z plane with the use of the corresponding density distribution in Fig. 2.

Results of the k-resolved measurements at a CO_2 laser energy of 11 J are summarized in Fig. 5 where we have plotted the time evolution as a function of position (density) and wave number. The greater wave numbers appear first in the critical-density region. The smaller wave numbers appear later in the subcritical region. This behavior is characteristic of low T_e/T_i ratio,[6] where different k values are unstable at different densities. This behavior is also consistent with an ion-acoustic instability driven by return current. In such a model one would expect the initial return current to be greatest on the high-density side so that the instability should be initiated at this position first. The fact that smaller wave numbers are excited later at subcritical density indicates that the instability is nonconvective and driven by a return current in this region which takes longer to build up.

The wave-number dependence on density is quite close to $k\lambda_D = 0.11$–0.12, under the assumption of a constant electron temperature ($T_e = 100$ eV) throughout. Agreement is good at low ($n/n_c \leq 0.6$) and high ($n/n_c = 2$) density where the width of the wave-number distribution is narrow ($\Delta k/k \simeq 5\%$). At densities near critical, the spectrum width is much greater ($\Delta k/k \geq 15\%$). At a background density of $n/n_c = 0.8$, fluctuations satisfying $k\lambda_D = 0.11$–0.12 are short lived with the higher wave numbers lasting twice as long. Profile modification, which is present at this laser energy level, can account for these last two effects. If we consider the wave-number distribution to peak at $k\lambda_D = 0.11$–0.12 independent of density as our data suggest, depression of the density profile tends to increase the peak wave number of the fluctuations and profile steepening to increase the width of the wave-number distribution at a

given location. We also note that simulations[4,5] show fluctuations peaking at $k\lambda_D = 0.1$ to extend from $n/n_c = 1$ to about $n/n_c = 0.6$.[4] This is also the subcritical density range where we observe fluctuations (Fig. 4). The wave-number distribution peaks much below the linear-theory[3] prediction of $k\lambda_D \simeq 0.7$ and is also lower than the nonlinear-theory prediction[5] of $k\lambda_D \simeq 0.35$ where the higher wave numbers are damped by trapped ions.

The absolute fluctuation level is $\delta n/n \simeq 15\%$ at a laser energy of 40 J. This fluctuation level (though not saturated with laser energy) corresponds to the (temporal) saturation level estimated by the wave-breaking model[3] for a temperature ratio $T_e/T_i = 4$. Saturation by scattering of phonons on ions[1] also limits the fluctuation level to $\delta n/n \simeq 10\%$ for long-wavelength fluctuations. Renormalization theory[5] predicts the same fluctuation level and parameter dependence as phonon-ion scattering if fast-ion production is not taken into account. Including this effect[5] reduces the level to $\delta n/n \simeq 10^{-3}$.

We acknowledge many fruitful discussions with T. W. Johnston and the collaboration of J. Sabbagh in performing Abel inversion of the interferograms. The assistance of R. Benesch in all phases of the experimental work and that of A. Avery in operating the CO_2 laser are also gratefully acknowledged.

[1]B. B. Kadomtsev, *Plasma Turbulence* (Academic, New York, 1965), p. 71; R. Z. Sagdeev and A. A. Galeev, in *Nonlinear Plasma Theory* (Benjamin, New York, 1969), p. 94; R. Z. Sagdeev, Rev. Mod. Phys. 51, 1 (1979).

[2]W. M. Manheimer, D. G. Colombant, and B. H. Ripin, Phys. Rev. Lett. 38, 1135 (1977); W. M. Manheimer and D. G. Colombant, Phys. Fluids 21, 1818 (1978).

[3]R. J. Faehl and W. L. Kruer, Phys. Fluids 20, 55 (1977).

[4]K. Estabrook, Phys. Rev. Lett. 47, 1396 (1981).

[5]W. Horton, D. I. Choi, and R. A. Koch, Phys. Fluids 22, 797 (1979), and Phys. Rev. A 14, 424 (1976); D. Biskamp and R. Chodura, Plasma Phys. Controlled Nucl. Fusion Res. 2, 265 (1971).

[6]W. M. Manheimer, Phys. Fluids 20, 265 (1977); D. G. Colombant and W. M. Manheimer, Phys. Fluids 23, 2512 (1980).

[7]H. C. Barr and T. J. M. Boyd, J. Plasma Phys. 27, 525 (1982).

[8]D. R. Gray, J. D. Kilkenny, M. S. White, P. Blyth, and D. Hull, Phys. Rev. Lett. 39, 1270 (1977); A. A. Offenberger, A. Ng, and L. Pitt, Phys. Rev. Lett. 40, 873 (1978); C. Stenz, thèse D.Sc., Université de Paris Sud, 1980 (unpublished).

[9]C. J. Walsh, H. A. Baldis, and R. G. Evans, Phys. Fluids 25, 2326 (1982).

[10]D. F. Dubois and M. V. Goldman, Phys. Rev. Lett. 14, 544 (1965).

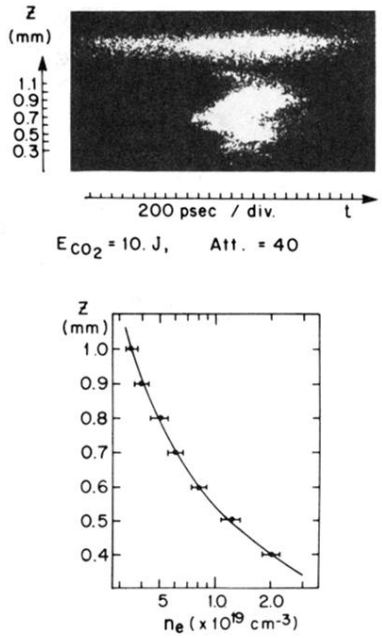

FIG. 2. Scattered signal as a function of distance from target (z) and time (t) as seen at the output of the streak camera. Attenuation (Att.) of the scattered signal is also indicated. The upper trace is the probe beam used to normalize the scattered power. The streak camera is triggered by the electrical pulse from the CO_2 shaping Pockels cells. This ensures a jitter less than 50 psec in the triggering of the streak camera with respect to the CO_2 laser pulse and allows time correlation between different shots. The associated measured background density profile is shown below.